Chapter 8

Polymerizable Materials for Diffractive Optical Elements Recording

Roberto Fernández Fernández,
Víctor Navarro Fuster,
Francisco J. Martínez Guardiola, Sergi Gallego Rico,
Andrés Márquez Ruiz, Cristian Neipp López,
Inmaculada Pascual Villalobos and
Augusto Beléndez Vázquez

Additional information is available at the end of the chapter

http://dx.doi.org/10.5772/intechopen.71511

Abstract

The technologies based on holographic and photonic techniques related to the optical storage and optical processing of information are rapidly evolving. One of the key points of this evolution are the new recording materials able to perform under the most specific situations and applications. In this sense, the importance of the photopolymers is growing spectacularly. This is mainly due to their versatility in terms of composition and design together with other interesting properties such as self-processing capabilities. In this chapter, we introduce the diffractive optical elements (DOE) generation in these materials and some of the most important parameters involved in this process. The deep knowledge of the material is essential to model its behavior during and after the recording process and we present different techniques to characterize the recording materials. We also present a 3D theoretical diffusion model able to reproduce and predict the experimental behavior of the recording process of any kind of DOE onto the photopolymers. The theoretical results will be supported by experimental analysis using a hybrid optical-digital setup, which includes a liquid crystal on silicon display. Besides this analysis, we study a method to improve the conservation and characteristics of these materials, an index-matching system.

Keywords: photopolymer, holography, diffractive optical elements, recording materials

1. Introduction

The holographic recording materials are traditionally used to record holograms, and they have been mainly studied and characterized for holographic applications [1–3]. Along with the evolution of photonics, communications and optical processing of information, the relevance, and capabilities of these materials to store any kind of phase or amplitude diffraction pattern, with good results also for low spatial frequencies, are surfacing [4–6]. At this point, the complete characterization of these materials for low spatial frequencies is decisive to design a material with the optimum characteristics for each specific application [7, 8].

The holographic recording materials change their properties when they are exposed to the light, and there are many examples of them, for example, the photographic emulsions [9], photochromic materials [10], dichromated gelatin [11], photorefractive materials [12], or photopolymers [13].

The last ones, photopolymers, are a very promising option, for example, for the development of holographic memories due to its high resolution and fidelity. The use of this recording material has spectacularly been increased because of its versatility at the time of changing their composition or design [14]. Moreover, they present high reliability, repeatability, and flexibility together with their tunable thickness, self-processing capabilities, and low cost. It is undeniable how those features set the photopolymers as one of the best holographic storage media and a good option for applications inside the diffractive optics and optical processing fields.

In these fields, one of the main drawbacks to be faced is the conservation of the element recorded into the photopolymer. In this sense, along this chapter, we will study the effects and improvements added by a coverplating together with an index-matching system. This system not only improves the lifetime of the material but also affects to the molecules diffusion inside the material.

2. Overview of the materials and DOE recording process

2.1. The recording materials

A photopolymer is a formulation based in an organic polymer sensitive to the light of certain wavelength. The basic formula is made of a sensitizer dye, an initiator to generate free radicals and one or more polymerizable monomers. These components are disposed in a matrix composed of a polymer such as poly(vinyl alcohol) (PVA), sodium polyacrylate, or vinyl chloride (PVC).

The basic way to record a DOE into a photopolymer, a phase media, is by refractive index modulation between the polymerized and nonpolymerized areas, which correspond to illuminated and nonilluminated areas, respectively [15].

A great variety of these materials can be developed based on a given monomer, a support matrix, a dye, and the rest of the components of the solution. These components and their concentration will affect the final properties of the photopolymer, as well as its applications.

The main factor is the binder, because it will determine the range of monomer, dye, and initiator to be used in the final compound.

In this chapter, all the results presented are based on three different materials: one of the most studied photopolymers, based on PVA and acrylamide (AA) as main monomers, which has demonstrated its high linearity and fidelity working in low- and high-spatial frequencies [4, 5]. Despite these good characteristics, the main drawback of this material is its high toxicity, mainly given by AA, which is known to be carcinogenic since many years. Also, it is known that the low environmental compatibility in terms of the low biodegradability of the devices is made of this material [16]. In this sense, our research group has developed a biocompatible photopolymer, called Biophotopol [17], which use sodium acrylate (NaAO) as a main monomer and has demonstrated to have a great dynamic range and high sensitivity together with its high biocompatibility and the main properties of the photopolymers such as the self-processing capabilities and low cost.

The third material used, polymer dispersed liquid crystal (PDLC), demonstrates how the versatility of the photopolymers can be improved by the inclusion of new components, like nanoparticles or dispersed liquid crystal (LC) molecules, in their formula [18, 19]. In this case, thanks to the addition of LC molecules, it is possible to fabricate polymers that change their optical properties by means of an external stimulus, in this case an electrical field. A hologram can be recorded into the material and then modulate its DE on real time thanks to the electrical field applied. The formulations of the different materials are shown in **Table 1**.

2.2. The photopolymerization reaction

The photopolymerization reaction (**Figure 1**) starts when the photopolymers are illuminated by light of certain wavelength, and the monomer starts to polymerize, causing a shrinkage on the illuminated areas, increasing the refractive index and decreasing the monomer concentration of these areas. This chemical compound gradient of the monomer, dye and radical generator causes a diffusion of the different components from the areas where the concentration is high, "dark areas" to the areas where the concentration has decreased, the "illuminated areas." This diffusion causes a decreasing of volume in the dark areas, and therefore, the volume of the illuminated areas is increased by incoming molecules, counteracting the shrinkage due to the polymerization process.

Material: PVA/AA-based photopolymer					
TEA (ml): 2.0	PVA (ml) (8%, w/v): 25	AA (g): 0.84	BMA (g): 0.2	YE (0.8%, w/v) (ml): 0.6	
Material: Biophotopol					
PVA (8%, w/v): 15	NaAO (M): 0.34	TEA (M): 0.15	PRF (M): 1.00×10^{-3}		
Material: PDLC (wt%)					
DPHPA: 48.8	BL036: 29.2	YEt: 0.1	NPG: 1.5	NVP: 16.4	OA: 4.4

Table 1. Formulation of different photopolymers used.

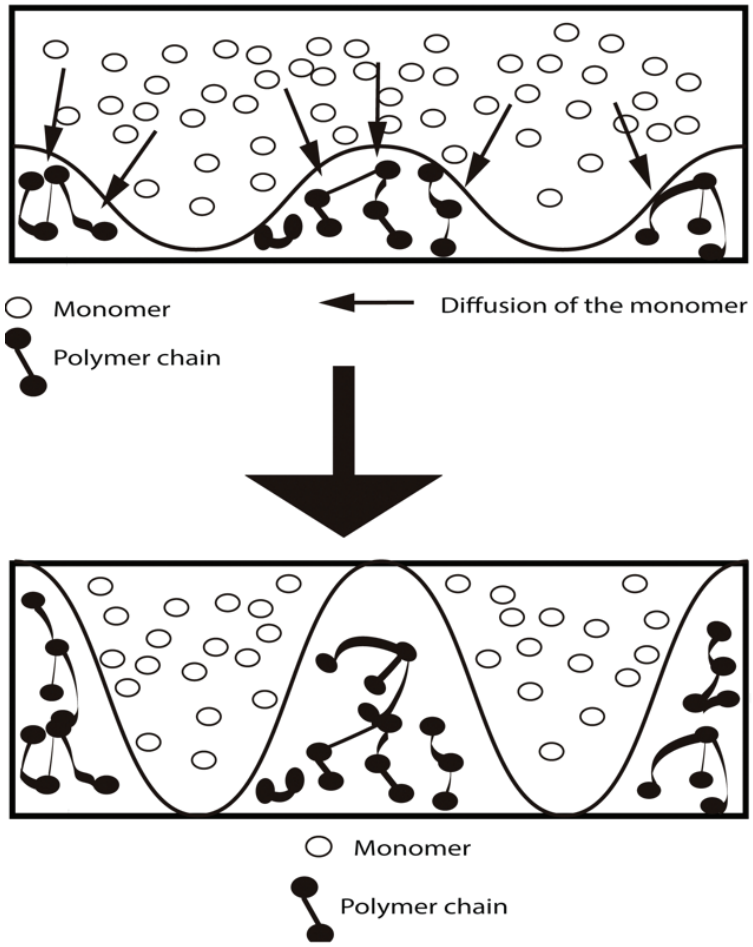

Figure 1. Representation of the formation of the hologram in a photopolymer.

The simplest DOE that can be recorded into a photopolymer is the sinusoidal profile, which can be obtained by the interference of two plane beams, controlling the period of the grating by changing the angle between the two beams. To record more complex DOE, it is necessary to control the shape of the incident beam to generate the desired profile. Nowadays, the advances on the spatial light modulators (SLMs) based on liquid crystal on silicon (LCoS) displays, thanks to the microelectronics technology, are allowing the production of commercial devices with resolutions higher than 4094 × 2464 (4 K) in the same size that of a conventional LCD screen. The use of this device in the optic setups allows the recording of an enormous variety of different complex DOEs with an active control of the function displayed by the LCD screen through a computer.

These complex profiles may suffer a smoothing of the profile due to different factors such as the cutoff frequency of the optical system, the cross talk between pixels, the finite size of the polymer chains, the diffusion of the monomer or the nonlinearity of the recording process. This deviation from the ideal profile depends on the R parameter, which indicates the relative importance of the photopolymerization with respect to the monomer diffusion:

$$R = \frac{DK_g^2}{F_R} \tag{1}$$

where D is the monomer diffusivity, F_R is the polymerization rate, and K_g is the grating number, related with the grating period Λ by means of $K_g = 2\pi/\Lambda$. At the time of modeling the behavior of these materials, there are many other parameters involved in the phase image formation process to consider, starting by the intensity and the fringes visibility, V. The importance of these parameters is analyzed by the relationship between polymerization rate and incident intensity.

$$F_R(t) = k_R(t) \cdot I^{\gamma}(x,z,t) = k_R\left(I_0\left[1 + Vcos\left(K_g x\right)\right]e^{-\alpha(t)z}\right)^{\gamma} \tag{2}$$

The $k_R(t)$ factor is the polymerization parameter, which indicates the speed of the photochemical reaction that takes place in the material and depends on the concentration and type of the substances involved and their media, $I(x,z,t)$ is the recording intensities' distribution, exponentially attenuated with depth due to the dye absorption (Beer's law [20]), α indicates this absorption (it decreases when the dye is consumed), V is the fringes visibility (typically 1), and γ represents the relationship between the polymerization rate and the recording intensity. This parameter usually takes values between 0.5 and 1, corresponding the value 0.5 to more liquid polymerizable systems and 1 to more solid systems.

To model the three-dimensional behavior of the monomer and polymer volume fractions, m and p, respectively, the following general equations can be used, where $\phi^{(m)}$ and $\phi^{(p)}$ are the monomer and polymer concentrations, respectively:

$$\frac{\partial\phi^{(m)}(x,z,t)}{\partial t} = \frac{\partial}{\partial x}D_m(t)\frac{\partial\phi^{(m)}(x,z,t)}{\partial x} + \frac{\partial}{\partial z}D_m(t)\frac{\partial\phi^{(m)}(x,z,t)}{\partial z} - F_R(x,z,t)\phi^{(m)}(x,z,t) \tag{3}$$

$$\frac{\partial\phi^{(p)}(x,z,t)}{\partial t} = F_R(x,z,t)\phi^{(m)}(x,z,t) \tag{4}$$

where D_m is the monomer diffusion inside the material, which decreases with time. To solve these differential equations, there are different methods. In the recording model used through this chapter, we have used the finite-difference method (FDM) to obtain a numerical solution.

Once we have measured the monomer and polymer concentrations, the refractive index of the photopolymeric layer can be calculated as a function of the volume fraction variations of each component using the Lorentz-Lorenz equation [21]:

$$\frac{n^2-1}{n^2+2}=\frac{n_m^2-1}{n_m^2+2}\phi^{(m)}+\frac{n_p^2-1}{n_p^2+2}\phi^{(p)}+\frac{n_b^2-1}{n_b^2+2}\left(1-\phi^{(m_0)}\right) \tag{5}$$

where $\phi^{(m_0)}$ is the average initial value for the monomer volume fraction, n_p is the polymer refractive index, n_m is the monomer refractive index, and n_b is the support matrix refractive index. These two last parameters can be measured using a refractometer, and the value of n_p can be obtained through zero-spatial frequency measurement technique [22].

The linearity in the material response can be studied in very low spatial frequencies to avoid the influence of the monomer diffusion in the diffractive image formation; the R parameter, described in Eq. (1), takes values higher than the ones obtained in holographic regime due to the high value of the spatial period.

The diffraction efficiency (DE) of the different diffracted orders in Fraunhofer domain is given by the Bessel functions [23]. **Figure 2** shows the behavior of the main four diffracted orders as a function of the phase shift. The comparison of this figure and the DE results obtained for certain material gives an approach of the linearity in the response of the material.

2.3. Influence of the index matching

As we mentioned in Section 1, one of the main drawbacks of the photopolymers is their conservation. In this sense, the inclusion of an index-matching system and coverplating not only improves the lifetime and conservation of the materials, but also allow us to measure the internal monomer diffusion [24]. This index-matching system allows us to clarify how the fast changes are measured in uncovered layers. Therefore, some authors observed in PVA/AA materials some fast changes on the surface [4]. They fitted this monomer diffusion around 10^{-7} cm^2/s. Some years late, Close et al. [25], using a coverplating and index-matching agent to

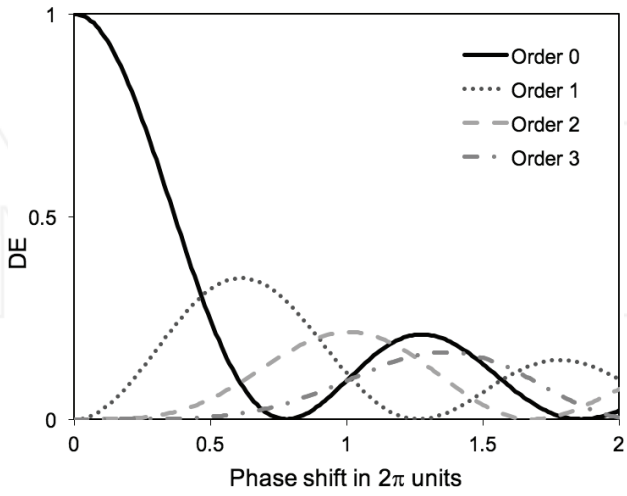

Figure 2. Diffraction efficiency of the main four orders of a sinusoidal grating as a function of the phase depth.

avoid the surface changes, measured the monomer diffusion inside the material around 10^{-10} cm^2/s. They also obtained the diffusion of other substances such as acetone inside the material, which lead us to make a distinction between the "apparent" diffusion of the surface, the first one, and the "real" diffusion, the internal monomer diffusion, the second one.

The thickness variations of the material play an important role in the DOEs formation at very low spatial frequency recording [5]. In DOEs recorded in materials without index matching, the transmitted beam has the information of the thickness and refractive index modulation mixed. By using the index-matching system (**Figure 3**), it is possible to study separately the changes produced by the refractive index variation. To achieve the index matching, we must choose a liquid with a refractive index very close to the mean of the polymer refractive index

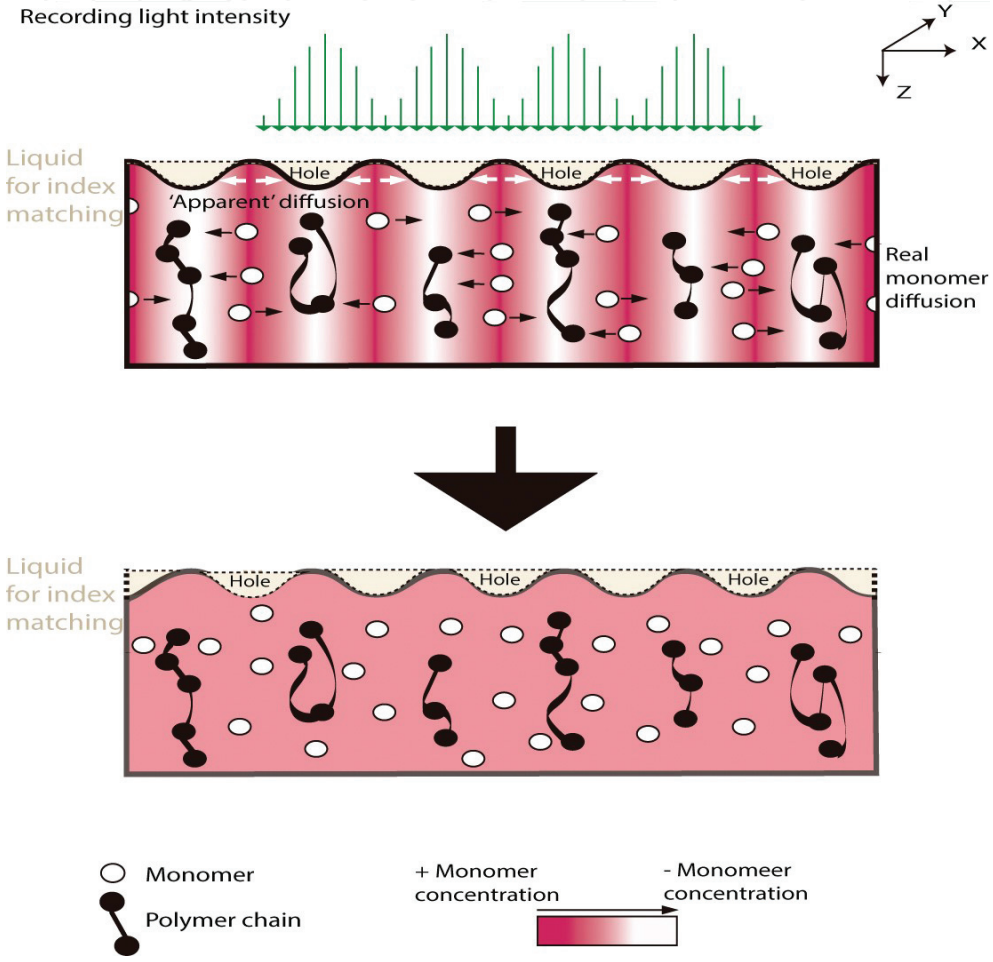

Figure 3. Diagram of a DOE recording using index-matching system. The so-called "apparent" diffusion is due to the recovering surface changes and the "real" diffusion is due to the internal monomer motion.

and not soluble with the photopolymer. When the shrinkage due to the polymerization takes place, this liquid will fill up the holes generated in the surface of the material, minimizing the diffractive effects due to the relief structure.

The value measured for uncovered layers due to this "apparent" diffusion is around 10^{-7} cm^2/s, which is not a suitable value to record complex DOEs with sharp profiles, due to the fast mass transfer, which produces a smoothening of these sharp profiles. For index-matched samples; this value is around 10^{-11} cm^2/s, suitable for complex structures recording. Thanks to the reduction of the mass transfer produced by the sealant, it is possible to record sharp profiles with insignificant smoothening of the profile.

2.3.1. Characterization of the different materials

To analyze the effects of this index-matching system, we use the setup shown in **Figure 4**; in this setup, we can distinguish two beams, the recording beam, provided by a solid-state Verdi laser (Nd-YVO4) with a wavelength of 532 nm (green light), at which the material exhibits maximum absorption, and the analyzing beam, provided by a He-Ne laser at a wavelength of 644 nm, at which the material is not sensitive.

The DOE to be recorded is provided by an LCoS SLM, placed along the recording arm of our setup and sandwiched between two polarizers (P), oriented to produce amplitude-mostly modulation. To obtain a linear response for each level of gray and good contrast, this device

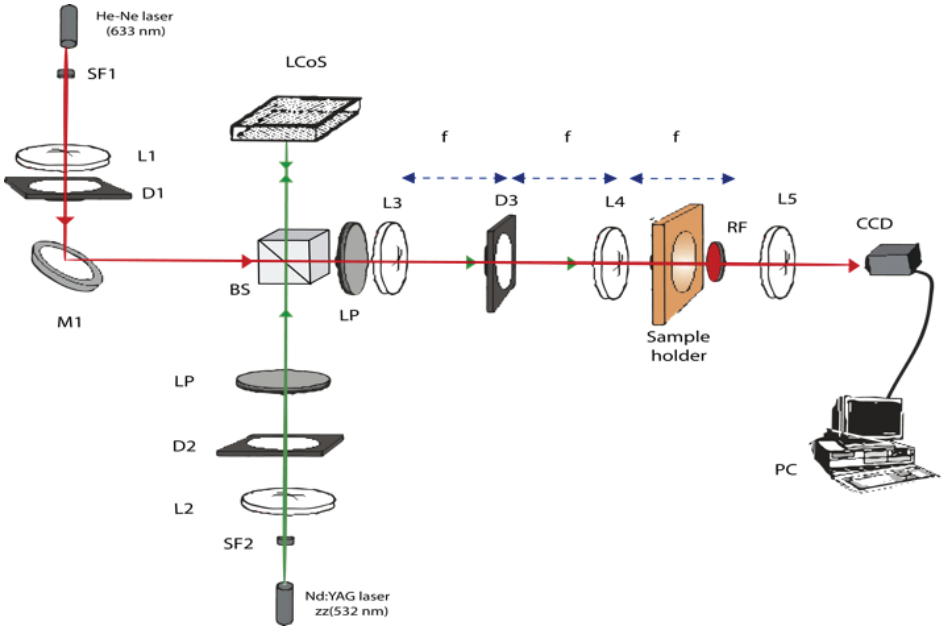

Figure 4. Experimental setup used to record and analyze in real time the DOEs formation on the photopolymers. Di, diaphragm; Li, lens; BS, beam splitter; SFi, spatial filter; LP, linear polarizer; and RF, red filter.

was characterized using the model proposed in [26]. Then, a 4F system images the intensity distribution generated by the SLM onto the recording material. The intensity of the recording beam is 0.25 mW/cm^2.

The analyzing arm, which allows us to study on real time the grating formation onto the photopolymer, was designed to collimate the light incident on the recording material, and a diaphragm (D1) was used to limit the aperture of the collimated beam. A nonpolarizing beam splitter (BS) split the beam in two within the same path. A red filter (RF) was placed behind the recording material to ensure that only the analyzing beam is incident on the CCD camera placed at the end of the setup. To separate the different diffraction orders, we placed a lens behind the material, obtaining the Fraunhofer diffraction pattern on the camera.

In **Figure 5**, the experimental DE of the four main orders for a sinusoidal grating with spatial period of 168 μm is shown. The sample has a thickness of 85 μm. We made two experiments, one without the coverplating and index-matching system (**Figure 5a**) and a second one using the index-matching system and coverplating (**Figure 5b**). It is noticeable how for longer exposure times, greater than 300 s, the phase modulation of both cases looks similar. In samples without index-matching, the recorded phase grating can be understood as the superposition of two phase gratings: a refractive index grating and a relief grating. It can be assumed that the effects of the last one are weaker for long exposure times. At these times, the fast diffusion through the surface in the uncovered sample has mitigated the effects of the relief grating. On the other hand, this relief grating causes that, in the case of the nonindex-matched sample, the maximum DE is achieved after 180 s, three times later that in the index-matched case. This is produced by the decrease in the phase modulation caused by the shrinkage, which is canceled at longer exposure times, as has already been said. In the experiments carried out for gratings with different spatial periods, we have observed that the behavior is similar. This is important for the recording of complex elements with different spatial frequencies mixed in their shapes such as diffractive lenses.

For the holographic regime, the diffusion times are very short and they do not exceed 0.1 s, which greatly hinders its measurement. Thus, to measure the species diffusion in frequencies around 1000 lines/mm, it is necessary to use indirect methods. At very low spatial frequencies,

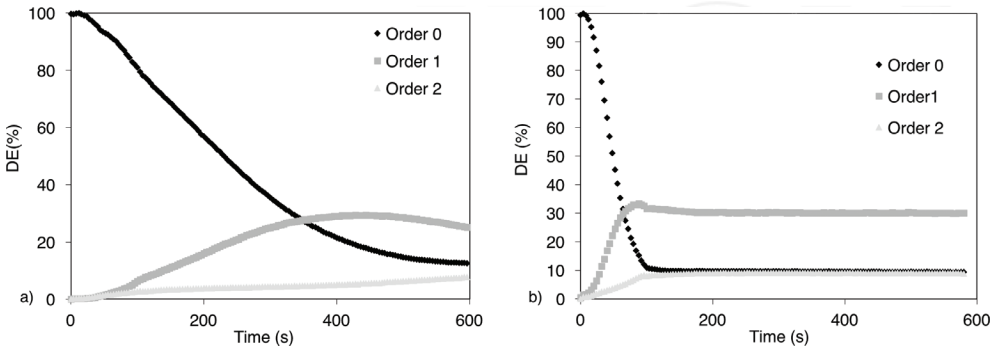

Figure 5. Experimental DE during recording of a grating with spatial period of 168 μm and thickness of 85 μm without index-matching system (a) and with index-matching system (b).

we can measure many diffracted orders to obtain information about the phase profile and its evolution after recording due to the diffusion. An interesting experiment is to measure the evolution of the DOE stored after recording. These variations are called in-dark evolution. In **Figure 6**, it can be appreciated the in-dark evolution of a nonindex-matched sample and an index-matched sample, exposing the sample during 50 s and shutting off the recording laser, analyzing the post exposure evolution of the DOE. For the nonindex-matched samples, the variation of the DEs is very fast in comparison with the index-matched ones. In the last case, it is noticeable how the two first orders remain practically constant after recording. The fitted values of the monomer diffusion in each case can be observed in **Figure 7**. We noted that the phase depth, $\Delta\phi$, becomes time independent after a time range, which goes from several minutes to a few days after exposure. Taking this into account, it is possible to follow the

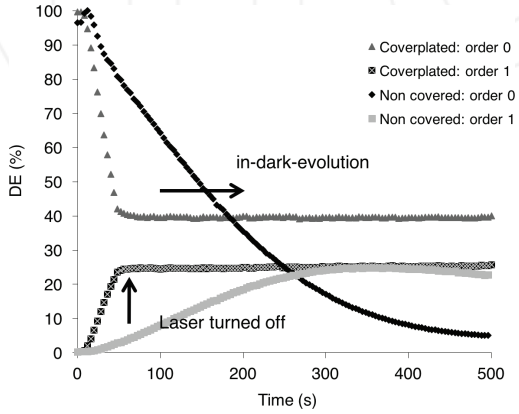

Figure 6. Experimental DE during 50 s recording of a sinusoidal grating of 168 μm in an 85 μm thickness index-matched and nonindex-matched samples and the in-dark evolution.

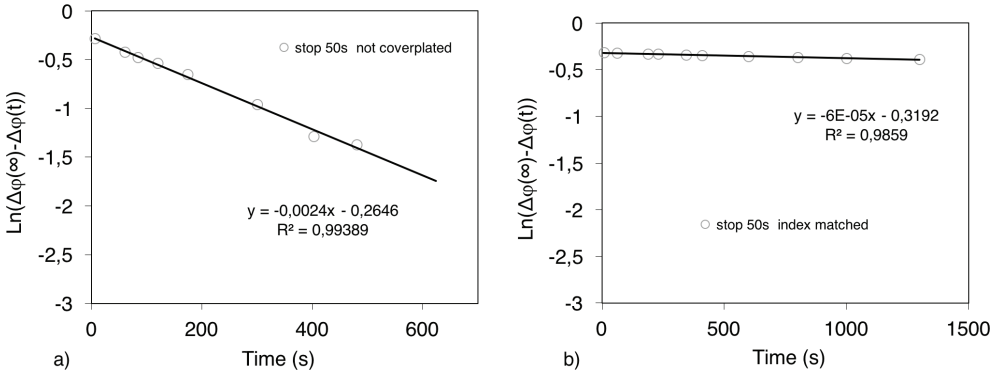

Figure 7. Fitting of the experimental values after 50 s of recording time a nonindex-matched sample (a) and index-matched sample (b).

procedure of [27] to obtain the "apparent" diffusion of this kind of materials, which depends on two variables: Λ, the grating period and τ, the characteristic time of monomer variation.

$$D = \frac{\Lambda^2}{4\pi^2\tau} \tag{6}$$

τ can be calculated by fitting the phase depth of the grating variation with time [6]. To obtain this value, we can use Fick's Law equation to describe species concentration after exposure and the fitting of the temporal variation for Δϕ:

$$\phi^{(i)}(x,t) = \phi_f^{(i)} + \Delta\phi^{(i)}(x)\exp\left(\frac{-t}{\tau}\right) \tag{7}$$

$$\Delta\varphi(\mathrm{x},\mathrm{t}) = V_m\Delta\phi^{(avg)}(x)\left(\exp\left(\frac{-t}{\tau}\right) - 1\right) \tag{8}$$

where the species modulation generated inside the photopolymer is represented by $\Delta\phi^{(i)}(\mathrm{x})$, $\phi_f^{(i)}$ is the average value of the residual species concentration, and $\Delta\phi^{(avg)}$ is the average for all molecules. This corresponds to the point at which monomer diffusion eventually stops due to a uniform monomer distribution. The molar volume of the monomer is represented by V_m and tends asymptotically (in practice in some minutes) to the value:

$$\Delta\varphi(\mathrm{x},\mathrm{t}\to\infty) = -V_m\Delta\phi^{(avg)}(x) \tag{9}$$

Thus, Eq. (8) can be simplified as:

$$\Delta\varphi(\mathrm{x},\mathrm{t}\to\infty) - \Delta\varphi(\mathrm{x},\mathrm{t}) = \Delta\varphi(\mathrm{x},\mathrm{t}\to\infty)\exp\left(\frac{-t}{\tau}\right) \tag{10}$$

And applying logarithm to both sides of the equation, we obtain:

$$\ln\left(\Delta\varphi(x,t\to\infty) - \Delta\varphi(x,t)\right) = \ln\left(\Delta\varphi(x,t\to\infty)\right) - \left(\frac{t}{\tau}\right) \tag{11}$$

The only assumption is that $\Delta\phi$ is proportional to $\Delta^{(avg)}$, which is reasonable for small polymer concentrations.

In **Figure 6**, it can be seen how the slope of the linear fitting for the nonindex-matched sample is almost two magnitude orders higher than the index-matched one. The diffusion measured for the last one is 3.5×10^{-10} cm^2/s, within the expected values for these materials. On the other hand, the "apparent" diffusion measured for the nonindex-matched sample is 1.6×10^{-8} cm^2/s. The differences between using or not the index-matching system are clear together with this separation between "apparent" and "real" diffusion. Using this index-matching system, it is possible to get a phase depth of 2π for PVA/AA samples of 105 μm without using any crosslinker. To get this, 2π phase depth modulation is very important as is needed by many applications related to the complex DOEs recording, such as blazed gratings or diffractive lenses [29, 30].

One of the methods to increase the phase depth is the inclusion of a crosslinker monomer. The role of this component is to increase the chain length and compaction by linking the polyacrylamide chains between them. Therefore, the polymerization rate, shrinkage, and refractive index are increased [30]. With the use of a crosslinker, it is possible to get the 2π phase depth in samples around 85 μm. In **Figure 8**, the effects of using N,N′-methylene-bis-acrylamide (BMA) as a crosslinker agent in the PVA/AA photopolymer formulation is shown. Comparing this figure with **Figure 2**, it is noticeable that the phase depth of 1.4·2π is reached after 200 s of exposure time in a sample of 95 μm thickness, a value substantially lower than the 105 μm needed for materials formulated without this crosslinker. Therefore, including agents such as BMA can drastically improve the material properties at very low spatial frequency recording.

The same analysis had been done for the Biophotopol green photopolymer, studying the effects of the index-matching system. Due to the similarities between this material and the PVA/AA-based one, Biophotopol also presents important relief structures formed during recording, avoiding the separate study of the refractive index distribution generated by polymerization. We have also studied the use of different crosslinker agents such as the already-mentioned BMA or the N,N′-(1,2-dihydroxyethylene) bisacrylamide (DHEBA), a highly environmental compatible crosslinker, which is also able to dissolve the NaAO, increasing the utility life of the samples up to 10 times, preventing the monomer crystallization [31]. **Figure 9** shows the experimental diffraction efficiency of a Biophotopol + DHEBA sample. In general, the results obtained are very similar to the ones obtained for the other photopolymers. In this case, the maximum phase depth obtained was around 1.4 π for a 90 μm sample. Therefore, assuming a linear behavior with thickness, a sample of around 128 μm will be required to achieve a phase depth of 2π. Regarding the monomer diffusion, the values obtained were around 10^{-10} cm^2/s, a bit slower compared to PVA/AA material.

At this point, it is also interesting to show the capabilities of the PDLC material to work with low spatial frequencies and develop tunable DOEs by means of an electrical field. The use of this material is very common for holographic regime, where it presents a high value of refractive index modulation providing DEs very close to 100% for optical thicknesses around 10 μm. The main drawback of this material is its high scattering. Regarding this factor, it is

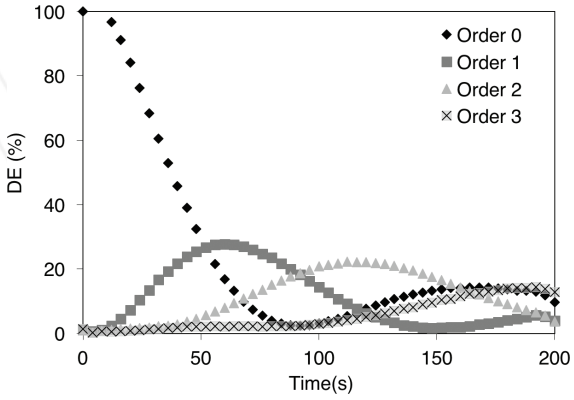

Figure 8. Experimental DE for the recording of a sinusoidal grating of 168 μm during 200 s of exposure time in an AA/PVA material with 95 μm thickness without the index-matching and coverplating system.

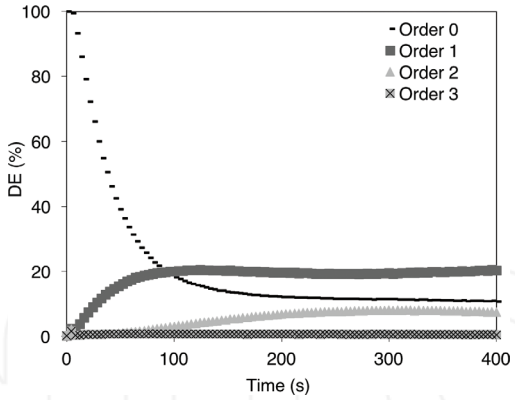

Figure 9. Experimental DE for the recording of a sinusoidal grating of 168 μm during 400 s of exposure time in an Biophotopol + DHEBA material with 90 μm thickness.

important to remark that this family of materials is always enclosed between indium tin oxide (ITO) glasses that make impossible to use the index-matching technique used in the other two materials. Thus, in this case, it is impossible to distinguish between "real" and "apparent" diffusion. The results obtained for the recording of a 168 μm period sinusoidal grating into a 30 μm thickness layer are shown in **Figure 10**. It can be seen how the phase depth of 2π can be achieved, but despite this, the fast values of diffusion, around 10^{-8} cm^2/s, together with the impossibility to distinguish the internal monomer diffusion from the "apparent" one make its selection difficult as a candidate to record low-frequency DOEs.

2.4. Simulation of the behavior of the materials

A model able to simulate the behavior of the material is a powerful tool to obtain the desired material or illumination parameters to fabricate a particular DOE. We have already introduced our recording model in Section 2.2. Based on the solving of the differential equations that

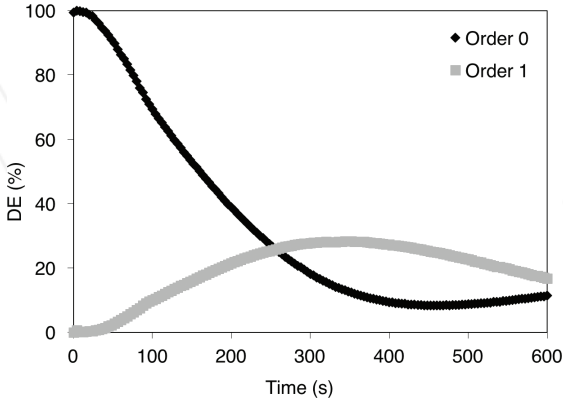

Figure 10. Experimental DE for the recording of a sinusoidal grating of 168 μm during 600 s of exposure time in a PDLC material with 30 μm thickness.

represents the behavior of the monomer and polymer volume fractions, it is possible to predict with fidelity how the different materials will behave during the DOEs recording. This model also includes the effects of the holes produced in the surface during polymerization process and analyzes both the hole and monomer diffusion separately [32].

Holes generation and its diffusion role in the model can be taken into account adding the following equations to the previously introduced, in Section 2.2:

$$\frac{\partial \phi^{(h)}(x,t)}{\partial t} = \frac{\partial}{\partial x} D_h(t) \frac{\partial \phi^{(h)}(x,z,t)}{\partial x} - K_h(x,t)\phi^{(m)}(x,t) \tag{12}$$

where $\phi^{(h)}$ represents the holes volume fraction and K_h is the holes rate generation, proportional to F_R, and D_h is the diffusion constant for holes. We assume that the holes are concentrated close to the surface, and their motion is along x direction, with the grating vector parallel to x-axis.

To check the capability of the recording model to simulate both the recording process on the material and the role of the sealant in this process, we recorded sinusoidal gratings in a PVA/AA material. The results obtained were compared with the simulation results, introducing in the model the parameters of the analyzed material. In **Figure 11** both the experimental results are shown that are compared with the simulation results of the DE of the main four orders of a sinusoidal grating with a period of 168 μm recorded into a PVA/AA material of 80 μm without (a) and with index matching (b). In both cases, the good agreement can be appreciated between the model and the experimental results. The results obtained are in line with the results shown previously, and the index-matched sample takes less time to reach the maximum DE due to the mitigation of the effects produced by the thickness variations.

The model is also capable to faithfully reproduce the postexposure evolution of the material in both index-matched and nonindex-matched samples. In **Figure 12**, it can be seen, apart from the good agreement between experimental and simulation results, how for the nonindex-

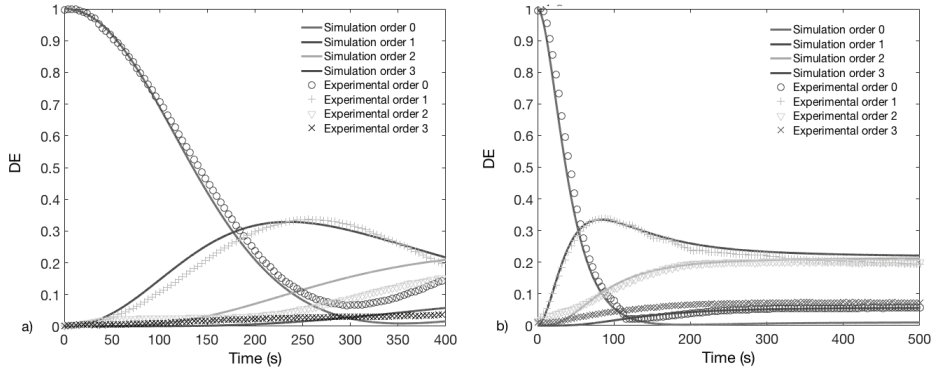

Figure 11. Comparison between experimental and simulated results of the main four orders of DE as a function of time for the recording of a sinusoidal grating of 168 μm in a PVA/AA material with 80 μm thickness, without index matching (a) and with it (b).

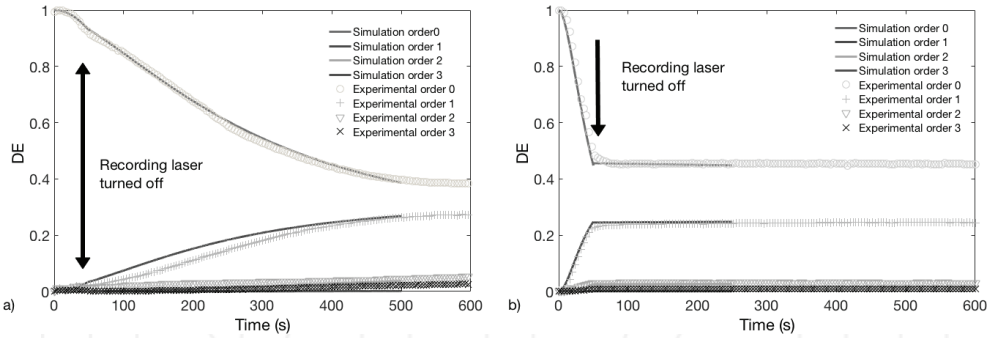

Figure 12. Comparison between experimental and simulated results of the postexposure evolution of the main four orders of DE as a function of time for the recording of a sinusoidal grating of 168 μm in a PVA/AA material with 80 μm thickness, without index matching (a) and with it (b).

matched sample (a) the DE continues changing after shutting of the recording beam due to the hole diffusion through the surface. These effects are not present in the index-matched sample (b), in which the DE evolution stops with the shutdown of the laser.

3. Recording of complex DOEs

3.1. Recording of blazed gratings

The lower monomer diffusion shown by the materials with index-matching system together with their capabilities of reaching 2π phase depth makes us able to explore the recording of more complex DOEs. One of these complex profiles is the blazed grating, a sharp profile with abrupt changes, which has many applications in communications and theoretically can reach DEs of 100% [28].

Taking into account the previous results of monomer diffusion, we attempt to store this kind of DOE in PVA/AA and Biophotopol materials. The value of D_0 tested for PDLC materials avoids the generation of sharp profiles on them. The recording model used is the one described in Section 2.2. In this case, the light intensity distribution during the recording process can be written as follows:

$$I = \frac{I_0}{\frac{1}{f_s \cdot \Delta_x} + 1} \tag{13}$$

where f_s is the period of the grating and I_0 is the maximum recording intensity.

The experimental setup has been described previously in Section 2.3.1. We placed the CCD camera in the material plane, and the image at this place and the intensity distribution of this image are shown in **Figure 13**. This figure shows a smoothening of the abrupt edges of the profile due to the low-pass filtering that the experimental setup introduces, especially due to

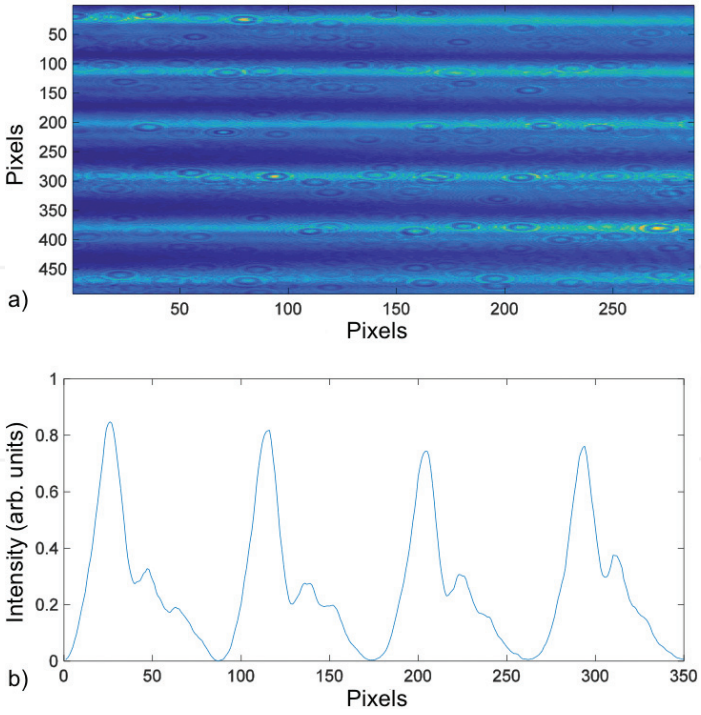

Figure 13. Image of a 672-μm blazed grating provided by the LCoS captured by the CCD at the material plane (a) and intensity profile across a vertical line of this image (b).

the diaphragm (D3) placed to eliminate the pixilation of the LCoS screen of the SLM. To improve the accuracy of the recording model, we introduced this recording intensity on it so that the model takes into account the low-pass filtering introduced by the experimental setup.

To analyze the response of the different materials and the capability of our model to predict the behavior of these materials, we perform different period gratings recording. First, we simulated the recording of this kind of DOE using our model to have an idea of the index-matching influence in both materials for different periods. Once we had a theoretical idea of the influence of index matching and period, we compared the simulations with the experimental results. **Figure 14** shows the simulated and the experimental DEs of a blazed grating of 672 μm recorded in a PVA/AA photopolymer 90 μm thick and a 336 μm one recorded in a Biophotopol photopolymer of 90 μm. It can be seen how the DE of the first order reaches a maximum of almost 70% after an exposure time of 150 s in the PVA/AA photopolymer and almost 55% in the Biophotopol one. Considering the low-pass filtering introduced by the setup, these are good results because we achieved near the maximum value of DE achievable taking into account this low-pass filtering. It is also noticeable that there is a good agreement between the simulation and the experimental results. The lower value of DE obtained for Biophotopol is due to the lower values of k_r and n_p of this family of photopolymers and can

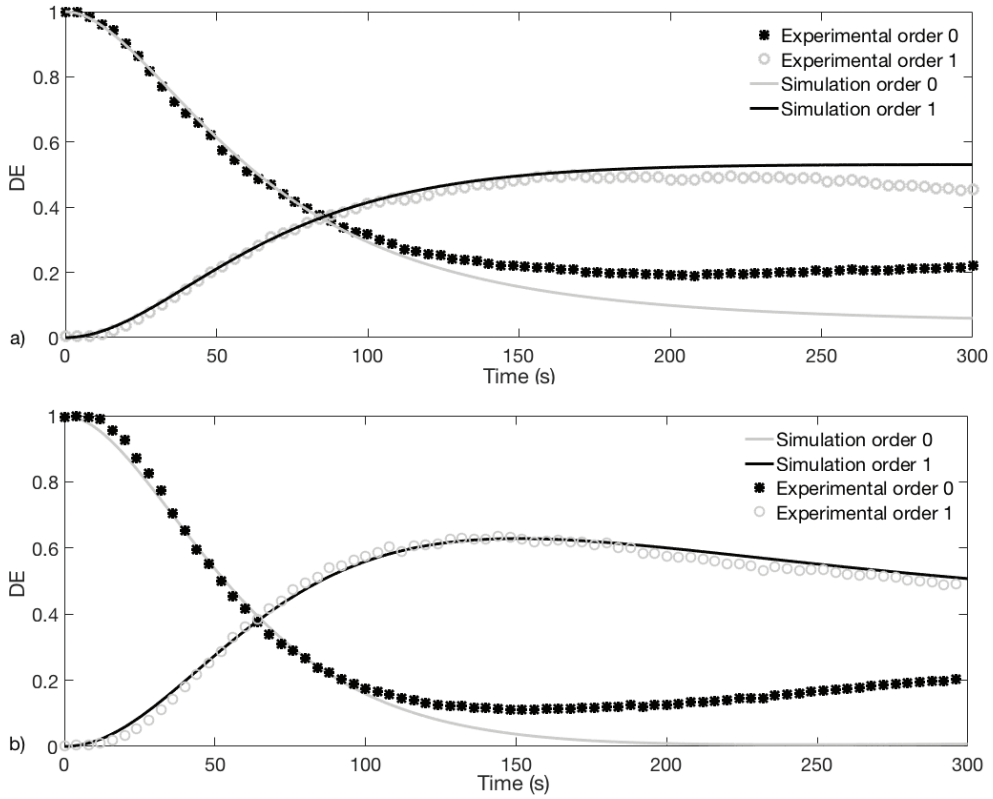

Figure 14. Comparison of the simulated and experimental DE of a 672 μm blazed grating recorded in a PVA/AA material (a) and a 336 μm blazed grating recorded in Biophotopol (b), both during an exposure time of 300 s.

be increased using thicker samples or higher concentrations of crosslinker in the final solution. For shorter period gratings recorded in the same kind of material, it is also appreciable a reduction of the maximum DE reached. This is due to the higher influence of the low-pass filtering at shorter spatial periods together with a higher diffusion.

In both cases and in the rest of the analysis carried out, the results present similarity independent of the spatial frequency of the grating, showing the low influence of the monomer diffusion at these spatial frequencies.

The recording model allows us to probe the capability of the materials to reach the 100% of DE without considering the low-pass filtering introduced by the experimental setup. This simulation is shown in **Figure 15**, where it can be seen how a DE of 100% could be reached for PVA/AA-based material and a DE of 97% for the Biophotopol one. The low-pass filtering introduced by the experimental setup means a reduction of over 20% of DE for both materials. This value is achieved at less exposure time than in the experiments by both materials due to the ideal recording intensity. It is also noticeable how in this ideal simulation, the PVA/AA-based

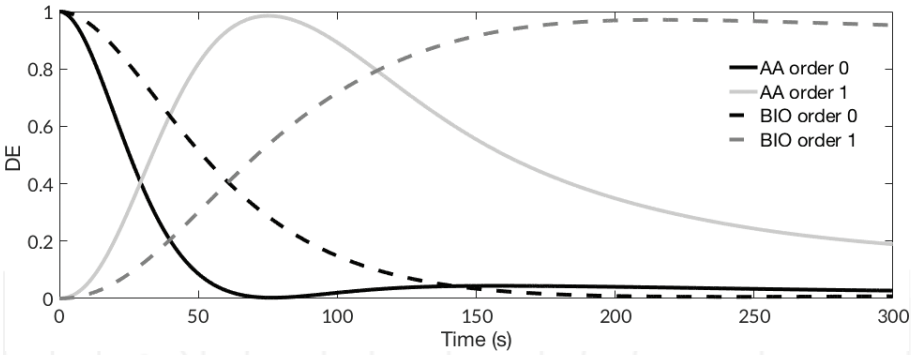

Figure 15. Simulation results of the DE as a function of time for PVA/AA and Biophotopol materials without taking into account the low-pass filtering introduced by the experimental setup.

material takes less time to reach the maximum DE than the Biophotopol due to the differences in n_p and k_r.

3.2. Diffractive lenses

The capabilities of the materials working with a complex profile such as blazed gratings have been proved obtaining near the maximum DE achievable taking into account the low-pass filtering introduced by the setup. Also, the recording model has demonstrated its fidelity reproducing the recording of this element in the different materials, with different spatial periods and considering the index-matching system and low-pass filtering.

Going further, another example of complex DOE to evaluate the model and materials capabilities is diffractive lenses. This DOE includes different spatial periods in its shape, being critical to avoid the smoothening of the profile and to achieve similar behavior for the different spatial periods.

The study of the recording of this kind of DOE has been made only for PVA/AA materials and Biophotopol for the same reasons of the blazed gratings. It is also important to remark that it is necessary to adapt the recording model to make it able to reproduce the cylindrical and spherical lenses formation in these materials. The two-spatial dimension equation shown in Section 2.2 can be applied to reproduce the cylindrical lenses behavior; nevertheless, it is necessary to add a new dimension, the "y" variable dimension, to simulate the case of a spherical lens recording [30]. Eqs. (3) and (4) remain as follows:

$$\frac{\partial \phi^{(m)}(x,y,z,t)}{\partial t} = \frac{\partial}{\partial z} D_m(t) \frac{\partial \phi^{(m)}(x,y,z,t)}{\partial z} + \frac{\partial}{\partial y} D_m(t) \frac{\partial \phi^{(m)}(x,y,z,t)}{\partial y} + \frac{\partial}{\partial x} D_m(t) \frac{\partial \phi^{(m)}(x,y,z,t)}{\partial x} - \\ - F_R(x,z,t)\phi^{(m)}(x,z,t) \tag{14}$$

$$\frac{\partial \phi^{(p)}(x,y,z,t)}{\partial t} = F_R(x,y,z,t)\phi^{(m)}(x,y,z,t) \tag{15}$$

http://dx.doi.org/10.5772/intechopen.71511

The recording intensity distribution is generated by the LCoS SLM in the amplitude regime, which, as in the previously shown experiments, is projected on the material to generate the corresponding phase element. This intensity distribution is defined in Eq. (16), where the phase depends on the quadratic value of the distance between the point and the lens centrum. This equation then is wrapped to 2π and normalized to the maximum value of intensity, I_0.

$$/(x,y) = exp\left[j\frac{\pi}{\lambda f}\left(x^2+y^2\right)\right] \tag{16}$$

In this equation, f is the focal length and λ represents the light wavelength. The intensity distribution of a 50 cm focal length lens generated using the SLM is shown in **Figure 16**.

The experimental setup used to record diffractive lenses is also the one already shown in **Figure 4**, with the particularity that in this case, L5 is not present as the lens recorded into the photopolymer is responsible for the focusing of the 633 nm wavelength beam. We imaged the point spread function (PSF) generated by this lens onto the CCD camera, controlling the magnification of the setup by means of the 4F system. The camera is also placed in the material plane to evaluate the intensity pattern imaged on the material. The image taken at this plane and the intensity profile across a horizontal line passing through the center of the lens are shown in **Figure 17**. We can see the characteristic ring structure with a decreasing spatial period as we move away from the center of the diffractive lens. Also, in the intensity profile image, it is noticeable the improvement of the profile with respect to ones presented using a transmissive LCD as SLM with a pixel size of 44 μm [33].

Using the recording model, it is possible to predict the refractive index distribution generated by the incident beam modulated by the SLM. Once we had obtained this refractive index distribution, we can apply the Fresnel propagation [34] to calculate the intensity distribution as a function of time. Thus, we can analyze the focalization of the lens and the optimum recording time to obtain a good focalization. In **Figure 18**, the results of the recording simulation can be seen for the recording of a 50 cm diffractive spherical lens in a PVA/AA material

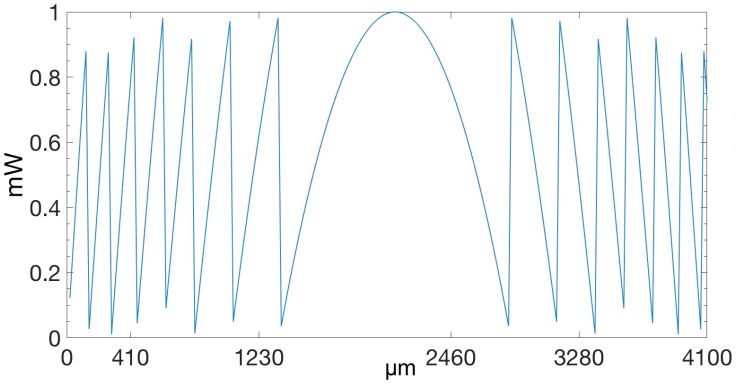

Figure 16. Horizontal cut of the theoretical intensity distribution of a 50 cm focal lens to be projected onto the photopolymer by the SLM.

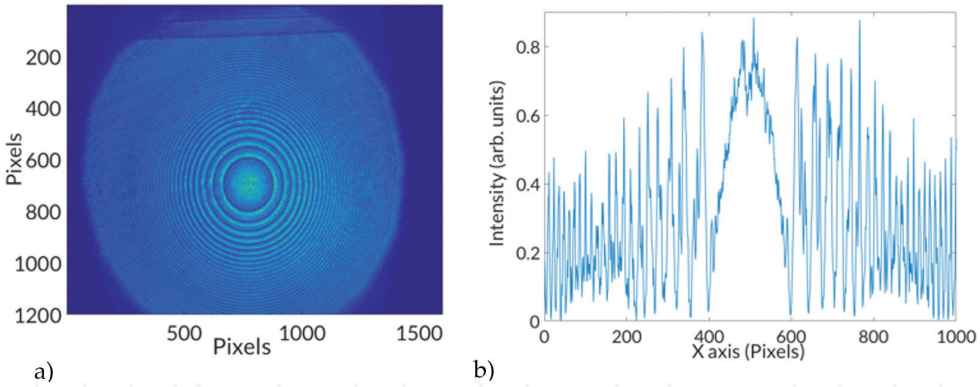

Figure 17. Image provided by the LCoS SLM at the material plane captured by the CCD camera (a) and intensity profile across a horizontal line passing through the center of the lens (b).

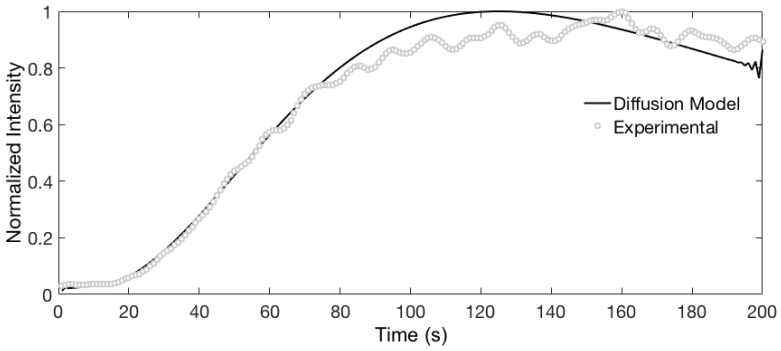

Figure 18. Intensity at the focal point as a function of time for a spherical lens f = 50 cm in a PVA/AA material of 95 μm.

with index matching compared to the experimental results, specifically the intensity at the focal point as a function of time. At this point, it is important to add that the simulated behavior exhibited by cylindrical and spherical lenses in the photopolymers used and different focal lenses is similar. Thus, the results shown correspond to the spherical one. In the figure, the good agreement is noticeable between the simulation and the experimental results, together with the good focalization power of the lenses. The model is also capable to predict the optimum recording time for the lenses in the different materials, as it will be shown in the following figures, and the decrease in the focal intensity. This occurs when the exposure time is longer than the optimum and the phase modulation overcomes 2π, as we chemically design the materials to obtain phase depth saturation slightly higher than 2π for the physical thickness used.

Thanks to the small pixel size of the LCoS screen of the SLM, it is possible to attempt to store shorter focal lenses, for example, 13 cm, to study the influence of the focal on the lenses

recording. **Figure 19** shows the comparison between the simulation and the experimental measurements of the intensity at the focal point as a function of time for two different focal lenses recorded in Biophotopol material. In this case, there is also a good agreement between the simulation and the experimental results. Both focal lenses present similar behavior than the one exhibited by the lens recorded in PVA/AA material. The lens with shorter focal takes less time to focalize, maybe due to the higher influence of the monomer diffusion.

3.2.1. Influence of the material parameters

At the beginning of the chapter, the importance of different parameters in the recording process was remarked. One of the most important aspects of having a recording model that takes into account many of these parameters is that we can study separately the influence of each one of them in the final DOE recorded. In this section, we will discuss the influence of one of these parameters, the internal monomer diffusion (D_0), as a sample of the model's capability. The influence of other parameters, such as the relationship between intensity and polymerization (γ) and the influence of the depth attenuation (α), can be consulted in Ref. [29]. We have studied the variation of each one of these parameters keeping the rest constant. This gives us the idea of which parameters are more important for the lens formation.

To check the influence of D_0, we have simulated different lenses with a range of monomer diffusivities from 3×10^{-8} to 3×10^{-11} cm^2/s and studied how the diffusion affects in the focal plane. **Figure 20** shows the intensity at the focal point for different internal monomer diffusivities. In this case, the intensity at the focal point for the two smallest values does not show any important difference. On the other hand, for both highest values of diffusivity, we appreciate a clear variation as it was expected. The increase in the monomer diffusivity has influence for these spatial frequencies for values higher than 3×10^{-10} cm^2/s. Below this value, the influence

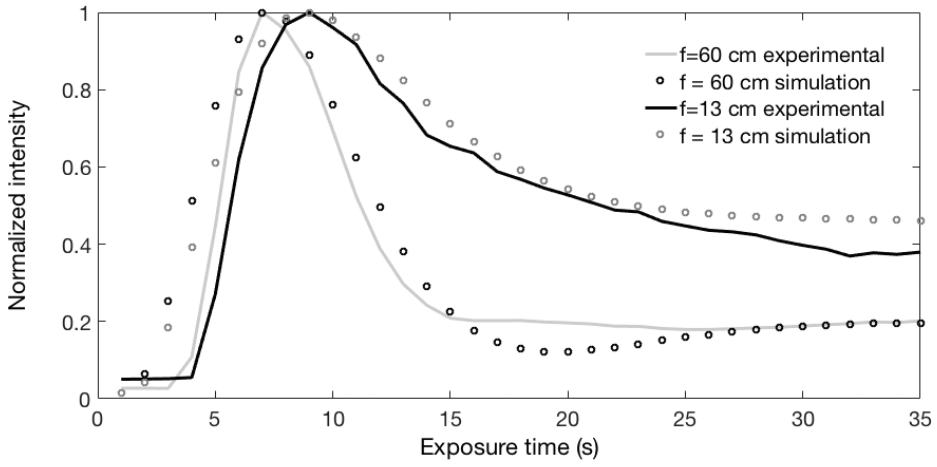

Figure 19. Comparison of the experimental results and the simulation of the intensity at the focal point for two different focal lengths (13 and 60 cm) of diffractive lenses recorded in Biophotopol material of 140 μm thickness.

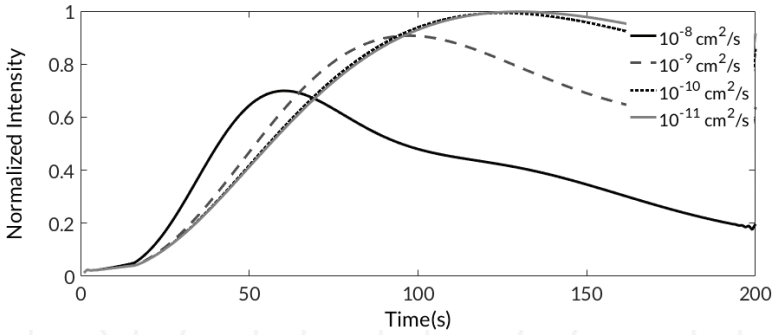

Figure 20. Intensity at the focal point as a function of time for different internal monomer diffusivities.

is low in the lens formation. Therefore, we assumed that for the PDLC material presented in a previous section, the results will not be as good as for the PVA/AA and Biophotopol materials.

4. Conclusions

In this chapter, we have presented a method to record low-frequency diffractive optical elements into photopolymers. This process is influenced by many parameters that we have introduced in a three-dimensional diffusion model to predict the phase image formation. Using this model together with different experimental measurements, we have developed an analysis of the requirements needed to achieve a phase modulation range of 2π in different families of materials. The results show the effectiveness and versatility of the recording model used. Thanks to this model, it is possible to predict the experimental behavior of the recording of any kind of DOE in the different photopolymers. The effectiveness of the model was validated by the experimental work carried out and based in the inclusion of an LCoS SLM. This device allows us to store any kind of DOE selected dynamically and analyze the influence of the different material properties during the recording.

Together with that, we have shown the effects of using the index-matching system, which apart from improving the conservation and lifetime of the recorded DOE, let us differentiate between the diffusion in the surface of the photopolymer and the internal diffusion. The lower values of diffusion obtained in the index-matched materials can be exploited to record sharp DOEs without significant smoothening of the refractive index profile.

Acknowledgements

We want to acknowledge the financial support from the Spanish Ministerio de Trabajo y Competitividad under projects FIS2014-56100-C2-1-P and FIS2015-66570-P and by the Generalitat Valenciana of Spain under project PROMETEOII/2015/015.

Author details

Roberto Fernández Fernández*, Víctor Navarro Fuster, Francisco J. Martínez Guardiola, Sergi Gallego Rico, Andrés Márquez Ruiz, Cristian Neipp López, Inmaculada Pascual Villalobos and Augusto Beléndez Vázquez

*Address all correspondence to: roberto.fernandez@ua.es

University Institute of Physics Applied to Sciences and Technologies, University of Alicante, Alicante, Spain

References

[1] Weiser MS, Bruder FK, Fäcke T, Hönel D, Jurbergs D, Rölle T. Self-processing, diffusion-based photopolymers for holographic applications. Macromolecular Symposia. 2010;**296**(1):133-137. DOI: 10.1002/masy.201051020

[2] Lechner MD. Photopolymers for optical memories and waveguides. In: Kuzmany H, Mehring M, Roth S, editors. Electronic Properties of Polymers and Related Compounds. Berlin, Heidelberg: Springer; 1985. DOI: 10.1007/978-3-642-82569-9_55

[3] Coufal HJ, Psaltis D, Sincerbox DT, editors. Holographic Data Storage. Berlin, Heidelberg: Springer; 2000. DOI: 10.1007/978-3-540-47864-5

[4] Baveba T, Naydenova I, Martin S, Toal V. Method for characterization of diffusion properties of photopolymerisable systems. Optics Express. 2008;**16**(12):8487-8497. DOI: 10.1364/OE.16.008487

[5] Close CE, Gleeson MR, Sheridan JT. Monomer diffusion rates in photopolymer material. Part I. Low spatial frequency holographic gratings. Journal of the Optical Society of America B. 2011;**28**(4):658-666. DOI: 10.1364/JOSAB.28.000658

[6] Gallego S, Márquez A, Ortuño M, Francés J, Marini S, Pascual I, Beléndez A. Surface relief model for without coverplating photopolymers. Optics Express. 2011;**19**(11):10896-10906. DOI: 10.1364/OE.19.010896

[7] Gallego S, Márquez A, Martínez-Guardiola FJ, Riquelme M, Fernández R, Pascual I, Beléndez A. Linearity in the response of photopolymers as optical recording media. Optics Express. 2013;**21**(9):10995-11008. DOI: 10.1364/OE.21.010995

[8] Zhao G, Mouroulis P. Diffusion model of hologram formation in dry photopolymers materials. Journal of Modern Optics. 1994;**41**(10):1929-1939. DOI: 10.1080/09500349414551831

[9] Bjelkhagen HI. Silver-Halide Recording Materials. 2nd ed. Berlin, Heidelberg: Springer; 1995. 441 p. DOI: 10.1007/978-3-540-70756-1

[10] Duncan RC, Staebler DL. Inorganic photochromic materials. In: Smith HM, editor. Holographic Recording Materials. Topics in Applied Physics. Vol. 20. Berlin, Heidelberg: Springer; 1977. p. 133-160. DOI: 10.1007/3-540-08293-X_45

[11] Chang BJ, Leonard CD. Dichromated gelatin for the fabrication of holographic optical elements. Applied Optics. 1979;**18**(14):2407-2417. DOI: 10.1364/AO.18.002407

[12] Bradley DDC, Gelsen OM. Comment on observation of the photorefractive effect in a polymer. Physical Review Letters. 1991;**67**:2589. DOI: 10.1103/PhysRevLett.67.2589

[13] Günter P. Coherent light amplification and optical phase conjugation with photorefractive materials. Journal de Physique Colloques. 1983;**44**:C2–141-C2–147. DOI: 10.1051/jphyscol:1983219

[14] Calvo ML, Cheben P. Photopolymerizable sol–gel nanocomposites for holographic recording. Journal of Optics A: Pure and Applied Optics. 2009;**11**(2):024009. DOI: 10.1088/1464-4258/11/2/024009

[15] Kveton M, Fiala P, Havranek A. Polymer holography in acrylamide-based recording material. In: Rosen J, editor. Holography, Research and Technologies. InTech; 2011. DOI: 10.5772/14564

[16] Hashimoto K, Aldridge WN. Biochemical studies on acrylamide, a neurotoxic agent. Biochemical Pharmacology. 1970;**19**(9):2591-2604. DOI: 10.1016/0006-2952(70)90009-2

[17] Ortuño M, Fernández E, Gallego S, Beléndez A, Pascual I. New photopolymer holographic recording material with sustainable design. Optics Express. 2007;**15**(19):12425-12435. DOI: 10.1364/OE.15.012425

[18] Hata E, Mitsube K, Momose K, Tomita Y. Holographic nanoparticle-polymer composites based on step-growth thiol-ene photopolymerization. Optical Materials Express. 2011;**1**(2):207-222. DOI: 10.1364/OME.1.000207

[19] Suzuki N, Tomita Y. Silica-nanoparticle-dispersed methacrylate photopolymers with net diffraction efficiency near 100%. Applied Optics. 2004;**43**(10):2125-2129. DOI: 10.1364/AO.43.002125

[20] Gallego S, Ortuño M, Neipp C, Márquez A, Kelly JV, Sheridan JT, Beléndez A, Pascual I. 3D behaviour of photopolymers as holographic recording material. In: Proc. SPIE 6252, Holography 2005: International Conference on Holography, Optical Recording, and Processing of Information; 9 June 2006; Varna, Bulgaria, SPIE; 2006. p. 62520B. DOI: 10.1117/12.676525

[21] Aubrecht I, Miler M, Koudela I. Recording of holographic diffraction gratings in photopolymers: Theoretical modelling and real-time monitoring of grating growth. Journal of Modern Optics. 1998;**45**(7):1465-1477. DOI: 10.1080/09500349808230641

[22] Gallego S, Márquez A, Méndez D, Neipp C, Ortuño M, Álvarez M, Fernández E, Beléndez A. Real-time interferometric characterization of a polyvinyl alcohol based photopolymer at the zero spatial frequency limit. Applied Optics. 2007;**46**(30):7506-7512. DOI: 10.1364/AO.46.007506

[23] Hariharan P. Optical Holography: Principles, Techniques and Applications. 2nd ed. Cambridge: Cambridge University Press; 1996. DOI: 10.1017/CBO9781139174039

[24] Fernández R, Gallego S, Márquez A, Francés J, Martínez FJ, Beléndez A. Influence of index matching on AA/PVA photopolymers for low spatial frequency recording. Applied Optics. 2015;**54**(11):3132. DOI: 10.1364/AO.54.003132

[25] Close CE, Gleeson MR, Mooney DA, Sheridan JT. Monomer diffusion rates in photopolymer material. Part II. High-frequency gratings and bulk diffusion. Journal of the Optical Society of America B. 2011;**28**(4):842-850. DOI: 10.1364/JOSAB.28.000842

[26] Martínez FJ, Márquez A, Gallego S, Ortuño M, Francés J, Pascual I, Beléndez A. Predictive capability of average Stokes polarimetry for simulation of phase multilevel elements onto LCoS devices. Applied Optics. 2015;**54**(6):1379-1386. DOI: 10.1364/AO.54.001379

[27] Gallego S, Márquez A, Marini S, Fernández E, Ortuño M, Pascual I. In dark analysis of PVA/AA materials at very low spatial frequencies: Phase modulation evolution and diffusion estimation. Optics Express. 2009;**17**(20):18279-18291. DOI: 10.1364/OE.17.018279

[28] Fernández R, Gallego S, Márquez A, Francés J, Navarro-Fuster V, Beléndez A. Blazed gratings recorded in absorbent photopolymers. Materials. 2016;**9**(3):195. DOI: 10.3390/ma9030195

[29] Fernández R, Gallego S, Márquez A, Francés J, Navarro-Fuster V, Pascual I. Diffractive lenses recorded in absorbent photopolymers. Optics Express. 2016;**24**(2):1559-1572. DOI: 10.1364/OE.24.001559

[30] Andrzejewska E. Photopolymerization kinetics of multi-functional monomers. Progress in Polymer Science. 2001;**26**(4):605-665. DOI: 10.1016/S0079-6700(01)00004-1

[31] Fernández R, Gallego S, Francés J, Pascual I, Beléndez A. Characterization and comparison of different photopolymers for low spatial frequency recording. Optical Materials. 2015;**44**(1):18-24. DOI: 10.1016/j.optmat.2015.02.025

[32] Gallego S, Fernández R, Márquez A, Ortuño M, Neipp C, Gleeson MR, Sheridan JT, Beléndez A. Two diffusion photopolymer for sharp diffractive optical elements recording. Optics Letters. 2015;**40**(14):3221-3224. DOI: 10.1364/OL.40.003221

[33] Marquez A, Gallego S, Ortuño M, Fernandez E, Alvarez ML, Belendez A, Pascual I. Generation of diffractive optical elements onto a photopolymer using a liquid crystal display. In: SPIE Proceedings 7717, Optical Modelling and Design, 77170D; 14 May 2010; Brussels, Belgium. SPIE; 2010. DOI: 10.1117/12.854786

[34] Goodman JW. Introduction to Fourier Optics. 2nd ed. New York: McGraw-Hill; 1987. 528 p

INTECH